

# Raman scattering study of NaFe<sub>0.53</sub>Cu<sub>0.47</sub>As

W.-L. Zhang,<sup>1,\*</sup> Y. Song,<sup>2</sup> W.-Y. Wang,<sup>2</sup> C.-D. Cao,<sup>2,3</sup> P.-C. Dai,<sup>2</sup> and G. Blumberg<sup>1,4,†</sup>

<sup>1</sup>Department of Physics & Astronomy, Rutgers University, Piscataway, New Jersey 08854, USA

<sup>2</sup>Department of Physics and Astronomy and Rice Center for Quantum Materials, Rice University, Houston, Texas 77005, USA

<sup>3</sup>Department of Applied Physics, Northwestern Polytechnical University, Xi'an 710072, China

<sup>4</sup>National Institute of Chemical Physics and Biophysics, Akadeemia tee 23, 12618 Tallinn, Estonia

(Dated: April 25, 2018)

We use polarization-resolved Raman scattering to study lattice dynamics in NaFe<sub>0.53</sub>Cu<sub>0.47</sub>As single crystals. We identify 4  $A_g$  phonon modes at 125, 172, 183 and 197  $\text{cm}^{-1}$ , and 4  $B_{3g}$  phonon modes at 101, 138, 173, 226  $\text{cm}^{-1}$ . The phonon spectra are consistent with the  $Ibam$  group, which confirms that the Cu and Fe atoms form a stripe order. The temperature dependence of the phonon spectra suggests weak electron-phonon and magneto-elastic interactions.

The parent compound of iron-pnictide superconductor, NaFeAs, is a bad metal. It exhibits a tetragonal to orthorhombic transition at 52 K, a paramagnetic to spin-density wave (SDW) transition at 41 K, and a superconducting transition at 23 K [1]. Doping copper into NaFeAs suppresses the orthorhombic and SDW order and enhances superconductivity [2–4]. Recently, it was found that heavy Cu substitution on the Fe site induces Mott-insulator-like behavior [5, 6]. The electronic properties of the heavily doped NaFe<sub>1-x</sub>Cu<sub>x</sub>As are similar to lightly doped cuprates [5, 7, 8].

For  $x > 0.44$  a long-range collinear antiferromagnetic (AFM) order with moment only on the Fe sites develops below 200 K. The moment increases with Cu concentration [6]. At the solubility limit near  $x = 0.5$ , new superlattice peaks appear in the TEM diffraction pattern, which are interpreted as the signature of Cu and Fe stripe order formation [6], as depicted in inset of Fig. 1. Compared to the parent NaFeAs compound in the tetragonal phase, the stripe-ordering of Cu and Fe in heavily-doped NaFe<sub>1-x</sub>Cu<sub>x</sub>As removes the lattice four-fold rotational symmetry and reduces the crystallographic space group from  $Fm\bar{3}m$  (point group  $D_{4h}$ ) to  $Ibam$  (point group  $D_{2h}$ ), making a structural analogue of the magnetic order in NaFeAs.

Here we present polarization-resolved Raman scattering study of the lattice dynamics for NaFe<sub>0.53</sub>Cu<sub>0.47</sub>As single crystals. Four  $A_g$  phonon modes at 125, 172, 183 and 197  $\text{cm}^{-1}$  and four  $B_{3g}$  phonon modes at 101, 138, 173, 226  $\text{cm}^{-1}$  are identified. The phonon spectra are consistent with the Fe/Cu stripe-ordered structure. All the observed phonons exhibit Lorentzian line shape. Across the AFM phase transition, no phonon anomaly is observed. The data suggests weak electron-phonon and magneto-elastic interaction.

NaFe<sub>1-x</sub>Cu<sub>x</sub>As single crystals were grown by self-flux method [6, 9]. The nominal Cu concentration was  $x = 0.85$ , which resulted in  $x = 0.47$  actual concentration [6].

The crystal belongs to  $Ibam$  space group at room temperature, as shown in the inset of Fig. 1. The crystallographic principle axis [001] of the  $Ibam$  group is along Fe(Cu) stripe direction. We define X, Y and Z axes along

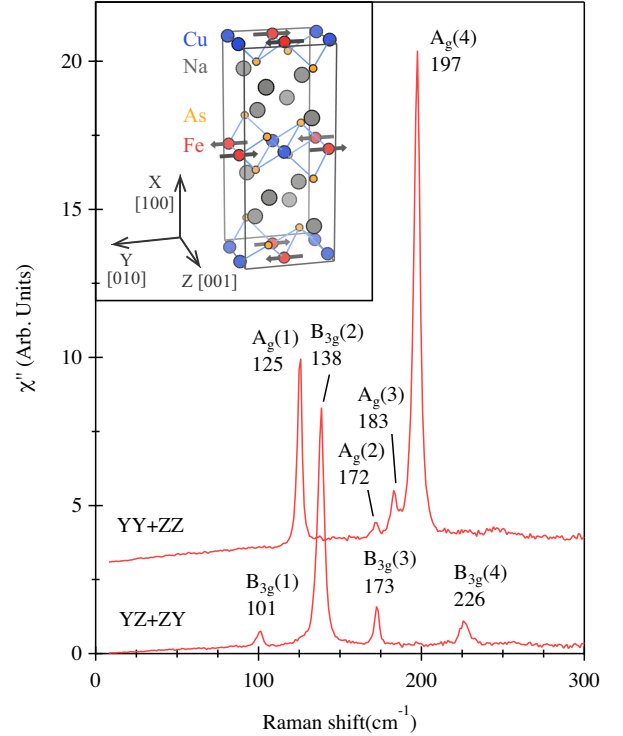


FIG. 1. Raman spectra of NaFe<sub>0.53</sub>Cu<sub>0.47</sub>As for scattering geometries YY+ZZ and YZ+ZY at 250 K measured with 1.9 eV excitation. Inset: NaFe<sub>0.5</sub>Cu<sub>0.5</sub>As unit cell with Cu and Fe collinear stripes. Arrows on the Fe sites mark the magnetic moments.

crystallographic [100], [010] and [001] axes and Y'/Z' along [011]/[0 $\bar{1}$ 1] directions (inset Fig. 2(a)).

There are 12 atoms in the primitive unit cell. Group theoretical analysis infers  $4A_g + 6B_{1g} + 4B_{2g} + 4B_{3g} + 2A_u + 4B_{1u} + 6B_{2u} + 6B_{3u}$  [10] symmetry decomposition of the 36 phonon modes at the Brillouin center  $\Gamma$  point. All the even  $g$  modes are Raman active. The irreducible representations and decomposition of the Raman active modes by symmetry are summarized in Table I.

Raman scattering measurements were performed in a quasi-back scattering setup from natural cleaved (100)

TABLE I.  $\Gamma$  point phonon mode decomposition and the selection rules for Raman-active modes in the  $Ib\bar{a}m$  group.

		Irreducible representations
Acoustic		$B_{1u}+B_{2u}+B_{3u}$
IR		$3B_{1u}+5B_{2u}+5B_{3u}$
Raman		$4A_g+6B_{1g}+4B_{2g}+4B_{3g}$
Silent		$2A_u$
Atom	Wyckoff position	Raman active modes
Na	8j	$2A_g+2B_{1g}+B_{2g}+B_{3g}$
Fe	4b	$B_{1g}+B_{2g}+B_{3g}$
Cu	4a	$B_{1g}+B_{2g}+B_{3g}$
As	8j	$2A_g+2B_{1g}+B_{2g}+B_{3g}$

surface. Samples were cleaved in a nitrogen-filled glove bag and immediately transferred to a continuous helium gas flow optical cryostat. We used 1.9 and 2.6 eV excitations from  $Kr^+$  laser, where the laser was focused into a  $50 \times 50 \mu m^2$  spot on the sample. The power was kept below 10 mW to minimize the laser heating. The estimated local heating was less than 5 K. All temperatures were corrected for laser heating.

The Raman scattering signal was analyzed by a triple-stage spectrometer with the spectral resolution setting at about  $2 \text{ cm}^{-1}$ . We used scattering geometries  $\mu\nu$  with  $\mu/\nu = Y, Z, Y'$  and  $Z'$ , where  $\mu\nu$  is short for  $\bar{X}(\mu\nu)X$  in Porto's notation. All spectra were corrected for the spectral response to obtain the Raman scattering intensity  $I_{\mu\nu}(\omega, T)$ . The Raman susceptibility  $\chi''_{\mu\nu}(\omega, T)$  was related to  $I_{\mu\nu}(\omega, T)$  by  $I_{\mu\nu}(\omega, T) = \chi''_{\mu\nu}(\omega, T)[1 + n(\omega, T)]$ , where  $n(\omega, T)$  is the Bose factor.

TABLE II. Raman tensor and selection rules for the Raman-active modes for  $D_{2h}$  group.

	$R_{A_g} = \begin{bmatrix} a & 0 & 0 \\ 0 & b & 0 \\ 0 & 0 & c \end{bmatrix}$		$R_{B_{1g}} = \begin{bmatrix} 0 & d & 0 \\ e & 0 & 0 \\ 0 & 0 & 0 \end{bmatrix}$
	$R_{B_{2g}} = \begin{bmatrix} 0 & 0 & f \\ 0 & 0 & 0 \\ g & 0 & 0 \end{bmatrix}$		$R_{B_{3g}} = \begin{bmatrix} 0 & 0 & 0 \\ 0 & 0 & h \\ 0 & i & 0 \end{bmatrix}$
(001) surface	XX	YY	XY/YX
	$A_g$	$a^2$	$b^2$
	$B_{1g}$	0	0
			$d^2/e^2$
(010) surface	XX	ZZ	XZ/ZX
	$A_g$	$a^2$	$c^2$
	$B_{2g}$	0	0
			$f^2/g^2$
(100) surface	YY/ZZ	YZ/ZY	Y'Y'/Z'Z' Y'Z'/Z'Y'
	$A_g$	$b^2/c^2$	0
			$(b+c)^2$
	$B_{3g}$	0	$(b-c)^2$
		$h^2/i^2$	$(h+i)^2$
			$(h-i)^2$

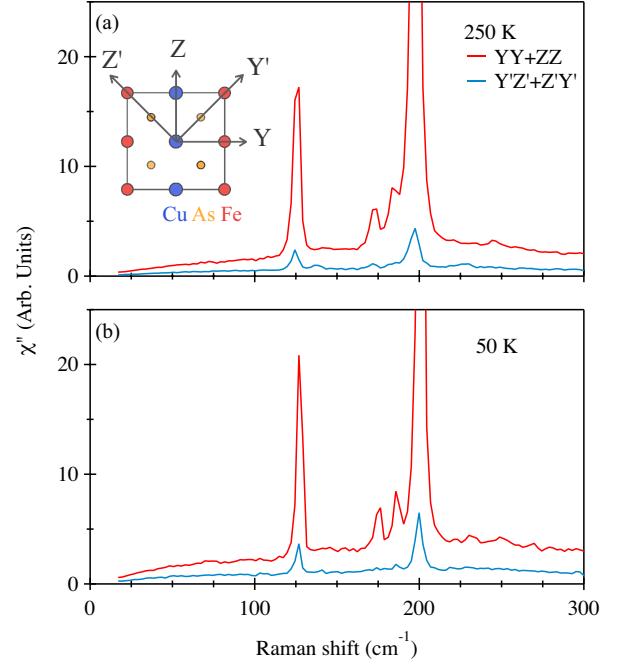


FIG. 2. Raman spectra of the  $A_g$  phonons for scattering geometries  $YY+ZZ$  and  $Y'Z'+Z'Y'$  at 250 K and 50 K measured with 2.6 eV laser excitation. inset: top view of the Fe-Cu-As layer and the  $YZ-Y'Z'$  coordinates.

In Table II we list the Raman tensor for  $D_{2h}$  group and the selection rule for experimentally accessible polarizations [11]. Due to twin structure [6], the collected signal from (100) surface is a superposition of Raman scattering intensities from two types of orthogonal domains. For example, the signal for parallel polarized scattering geometry along the crystallographic axes contains the intensity from  $YY$  geometry for one type of domain and  $ZZ$  geometry for the other type of domain. We denote this scattering geometry as  $YY+ZZ$ . Similarly, cross polarized signal along the crystallographic axes contains contributions from  $YZ$  and  $ZY$  geometries, is denoted  $YZ+ZY$ , and cross polarized signal along the diagonal directions contains contributions from  $Y'Z'$  and  $Z'Y'$  scattering geometries, is denoted  $Y'Z'+Z'Y'$ .

Following Table II, we assign all phonons that appear in the  $YY+ZZ$  geometry to the  $A_g$  symmetry modes, and those appear in the  $YZ+ZY$  geometry to the  $B_{3g}$  modes.

Fig. 1 shows the Raman response in  $NaFe_{0.53}Cu_{0.47}As$  at 250 K for  $YY+ZZ$  and  $YZ+ZY$  scattering geometries. We identify all the  $A_g$  and  $B_{3g}$  phonon modes predicted by group theory: four  $A_g$  symmetry modes at 125, 172, 183 and 197  $\text{cm}^{-1}$ , and four  $B_{3g}$  symmetry modes at 101, 138, 173, and 226  $\text{cm}^{-1}$ . All modes show symmetric line shape.

We note that at the same frequency as the  $A_g$  phonon modes, some modes with weaker intensity are also observed for the  $Y'Z'+Z'Y'$  geometry (Fig. 2). The inten-

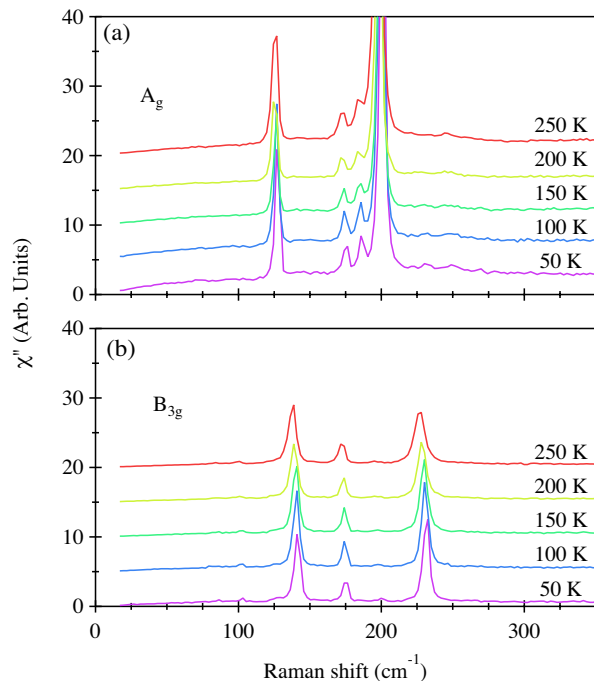


FIG. 3. Temperature dependent  $A_g$  and  $B_{3g}$  Raman spectra of  $\text{NaFe}_{0.53}\text{Cu}_{0.47}\text{As}$  measured with 2.6 eV laser excitation.

sity of the *leaking* modes is about 10% of the  $A_g$  phonon intensity in the YY+ZZ geometry, which is much higher than the experimental uncertainty. Similar *leakage* of the full symmetric phonon mode into cross polarized scattering geometry was reported for pristine  $\text{NaFeAs}$  crystals in the orthorhombic phase [12, 13], therefore, we attribute such *leakage* to the lowering of the crystallographic point group symmetry. Based on the Raman scattering selection rules, we deduce that the *leakage* intensity is proportional to  $(b - c)^2$  (Table I), which is a measurement of anisotropic electronic properties between Y and Z directions [14]. The observation of the *leakage* is consistent with formation of a long range stripe order.

In Fig. 3 we show temperature dependence of the Raman spectra for  $A_g$  (YY+ZZ) and  $B_{3g}$  (YZ+ZY) symmetry channels between 250 and 50 K. The number and the line shape of the phonon modes do not change across the AFM phase transition at 200 K, suggesting weak electron-phonon and magneto-elastic interaction.

In summary, we present polarization-resolved Raman scattering study of  $\text{NaFe}_{0.53}\text{Cu}_{0.47}\text{As}$  single crystals. We observe four  $A_g$  and four  $B_{3g}$  phonon modes at 125, 172, 183, 197  $\text{cm}^{-1}$  and 101, 138, 173, 226  $\text{cm}^{-1}$ , respectively. The results are consistent with the  $Ibam$  group symmetry structure where Fe/Cu atoms form stripe order. No phonon anomaly is observed across the magnetic phase transition between 250 to 50 K, suggesting weak electron-

phonon and magneto-elastic interaction.

The work at Rutgers is supported by the U.S. Department of Energy, Office of Basic Energy Sciences, Division of Materials Sciences and Engineering under contract No. DE-SC0005463. The work at Rice is supported by the U.S. Department of Energy, Office of Basic Energy Sciences under contract No. DE-SC0012311 and Robert A. Welch Foundation Grant No. C-1839.

\* wz131@physics.rutgers.edu

† girsh@physics.rutgers.edu

- [1] G. F. Chen, W. Z. Hu, J. L. Luo, and N. L. Wang, *Phys. Rev. Lett.* **102**, 227004 (2009).
- [2] J. D. Wright, T. Lancaster, I. Franke, A. J. Steele, J. S. Möller, M. J. Pitcher, A. J. Corckett, D. R. Parker, D. G. Free, F. L. Pratt, P. J. Baker, S. J. Clarke, and S. J. Blundell, *Phys. Rev. B* **85**, 054503 (2012).
- [3] A. F. Wang, J. J. Lin, P. Cheng, G. J. Ye, F. Chen, J. Q. Ma, X. F. Lu, B. Lei, X. G. Luo, and X. H. Chen, *Phys. Rev. B* **88**, 094516 (2013).
- [4] G. Tan, Y. Song, R. Zhang, L. Lin, Z. Xu, L. Tian, S. Chi, M. K. Graves-Brook, S. Li, and P. Dai, *Phys. Rev. B* **95**, 054501 (2017).
- [5] C. Ye, W. Ruan, P. Cai, X. Li, A. Wang, X. Chen, and Y. Wang, *Phys. Rev. X* **5**, 021013 (2015).
- [6] Y. Song, Z. Yamani, C. Cao, Y. Li, C. Zhang, J. S. Chen, Q. Huang, H. Wu, J. Tao, Y. Zhu, W. Tian, S. Chi, H. Cao, Y.-B. Huang, M. Dantz, T. Schmitt, R. Yu, A. H. Nevidomskyy, E. Morosan, Q. Si, and P. Dai, *Nat. Commun.* **7**, 13879 (2016).
- [7] C. E. Matt, N. Xu, B. Lv, J. Ma, F. Bisti, J. Park, T. Shang, C. Cao, Y. Song, A. H. Nevidomskyy, P. Dai, L. Patthey, N. C. Plumb, M. Radovic, J. Mesot, and M. Shi, *Phys. Rev. Lett.* **117**, 097001 (2016).
- [8] A. Charnukha, Z. P. Yin, Y. Song, C. D. Cao, P. Dai, K. Haule, G. Kotliar, and D. N. Basov, *Phys. Rev. B* **96**, 195121 (2017).
- [9] M. A. Tanatar, N. Spyrison, K. Cho, E. C. Blomberg, G. Tan, P. Dai, C. Zhang, and R. Prozorov, *Phys. Rev. B* **85**, 014510 (2012).
- [10] E. Kroumova, M. Aroyo, J. Perez-Mato, A. Kirov, C. Capillas, S. Ivantchev, and H. Wondratschek, *Phase Transit.* **76**, 155 (2003).
- [11] M. Klein, "Resonance phenomena," in *Light Scattering in Solids II*, Chap. 2, pp. 45–49.
- [12] V. K. Thorsmølle, M. Khodas, Z. P. Yin, C. Zhang, S. V. Carr, P. Dai, and G. Blumberg, *Phys. Rev. B* **93**, 054515 (2016).
- [13] S.-F. Wu, W.-L. Zhang, V. K. Thorsmølle, G. F. Chen, G. T. Tan, P. C. Dai, Y. G. Shi, C. Q. Jin, T. Shibauchi, S. Kasahara, Y. Matsuda, A. S. Sefat, H. Ding, P. Richard, and G. Blumberg, ArXiv e-prints (2017), [arXiv:1712.01896](https://arxiv.org/abs/1712.01896).
- [14] S.-F. Wu, W.-L. Zhang, L. Li, H.-B. Cao, H.-H. Kung, A. S. Sefat, H. Ding, P. Richard, and G. Blumberg, ArXiv e-prints (2017), [arXiv:1712.01903](https://arxiv.org/abs/1712.01903).